

$W\gamma$ production and limits on anomalous $WW\gamma$ couplings in $p\bar{p}$ collisions at $\sqrt{s} = 1.96$ TeV

V.M. Abazov,³⁴ B. Abbott,⁷² B.S. Acharya,²⁸ M. Adams,⁴⁸ T. Adams,⁴⁶ G.D. Alexeev,³⁴ G. Alkhalaf,³⁸ A. Alton,^{a,60} G. Alverson,⁵⁹ G.A. Alves,² M. Aoki,⁴⁷ M. Arov,⁵⁷ A. Askew,⁴⁶ B. Åsman,⁴⁰ S. Atkins,⁵⁷ O. Atramentov,⁶⁴ K. Augsten,⁹ C. Avila,⁷ J. BackusMayes,⁷⁹ F. Badaud,¹² L. Bagby,⁴⁷ B. Baldin,⁴⁷ D.V. Bandurin,⁴⁶ S. Banerjee,²⁸ E. Barberis,⁵⁹ P. Baringer,⁵⁵ J. Barreto,³ J.F. Bartlett,⁴⁷ U. Bassler,¹⁷ V. Bazterra,⁴⁸ A. Bean,⁵⁵ M. Begalli,³ M. Begel,⁷⁰ C. Belanger-Champagne,⁴⁰ L. Bellantoni,⁴⁷ S.B. Beri,²⁶ G. Bernardi,¹⁶ R. Bernhard,²¹ I. Bertram,⁴¹ M. Besançon,¹⁷ R. Beuselinck,⁴² V.A. Bezzubov,³⁷ P.C. Bhat,⁴⁷ V. Bhatnagar,²⁶ G. Blazey,⁴⁹ S. Blessing,⁴⁶ K. Bloom,⁶³ A. Boehnlein,⁴⁷ D. Boline,⁶⁹ E.E. Boos,³⁶ G. Borissov,⁴¹ T. Bose,⁵⁸ A. Brandt,⁷⁵ O. Brandt,²² R. Brock,⁶¹ G. Brooijmans,⁶⁷ A. Bross,⁴⁷ D. Brown,¹⁶ J. Brown,¹⁶ X.B. Bu,⁴⁷ M. Buehler,⁴⁷ V. Buescher,²³ V. Bunichev,³⁶ S. Burdin,^{b,41} T.H. Burnett,⁷⁹ C.P. Buszello,⁴⁰ B. Calpas,¹⁴ E. Camacho-Pérez,³¹ M.A. Carrasco-Lizarraga,⁵⁵ B.C.K. Casey,⁴⁷ H. Castilla-Valdez,³¹ S. Chakrabarti,⁶⁹ D. Chakraborty,⁴⁹ K.M. Chan,⁵³ A. Chandra,⁷⁷ E. Chapon,¹⁷ G. Chen,⁵⁵ S. Chevalier-Théry,¹⁷ D.K. Cho,⁷⁴ S.W. Cho,³⁰ S. Choi,³⁰ B. Choudhary,²⁷ S. Cihangir,⁴⁷ D. Claes,⁶³ J. Clutter,⁵⁵ M. Cooke,⁴⁷ W.E. Cooper,⁴⁷ M. Corcoran,⁷⁷ F. Couderc,¹⁷ M.-C. Cousinou,¹⁴ A. Croc,¹⁷ D. Cutts,⁷⁴ A. Das,⁴⁴ G. Davies,⁴² K. De,⁷⁵ S.J. de Jong,³³ E. De La Cruz-Burelo,³¹ F. Déliot,¹⁷ M. Demarteau,⁴⁷ R. Demina,⁶⁸ D. Denisov,⁴⁷ S.P. Denisov,³⁷ S. Desai,⁴⁷ C. Deterre,¹⁷ K. DeVaughan,⁶³ H.T. Diehl,⁴⁷ M. Diesburg,⁴⁷ P.F. Ding,⁴³ A. Dominguez,⁶³ T. Dorland,⁷⁹ A. Dubey,²⁷ L.V. Dudko,³⁶ D. Duggan,⁶⁴ A. Duperrin,¹⁴ S. Dutt,²⁶ A. Dyshkant,⁴⁹ M. Eads,⁶³ D. Edmunds,⁶¹ J. Ellison,⁴⁵ V.D. Elvira,⁴⁷ Y. Enari,¹⁶ H. Evans,⁵¹ A. Evdokimov,⁷⁰ V.N. Evdokimov,³⁷ G. Facini,⁵⁹ T. Ferbel,⁶⁸ F. Fiedler,²³ F. Filthaut,³³ W. Fisher,⁶¹ H.E. Fisk,⁴⁷ M. Fortner,⁴⁹ H. Fox,⁴¹ S. Fuess,⁴⁷ A. Garcia-Bellido,⁶⁸ G.A. García-Guerra,^{c,31} V. Gavrilov,³⁵ P. Gay,¹² W. Geng,^{14,61} D. Gerbaudo,⁶⁵ C.E. Gerber,⁴⁸ Y. Gershtein,⁶⁴ G. Ginther,^{47,68} G. Golovanov,³⁴ A. Goussiou,⁷⁹ P.D. Grannis,⁶⁹ S. Greder,¹⁸ H. Greenlee,⁴⁷ Z.D. Greenwood,⁵⁷ E.M. Gregores,⁴ G. Grenier,¹⁹ Ph. Gris,¹² J.-F. Grivaz,¹⁵ A. Grohsjean,¹⁷ S. Grünendahl,⁴⁷ M.W. Grünewald,²⁹ T. Guillemin,¹⁵ G. Gutierrez,⁴⁷ P. Gutierrez,⁷² A. Haas,^{d,67} S. Hagopian,⁴⁶ J. Haley,⁵⁹ L. Han,⁶ K. Harder,⁴³ A. Harel,⁶⁸ J.M. Hauptman,⁵⁴ J. Hays,⁴² T. Head,⁴³ T. Hebbeker,²⁰ D. Hedin,⁴⁹ H. Hegab,⁷³ A.P. Heinson,⁴⁵ U. Heintz,⁷⁴ C. Hensel,²² I. Heredia-De La Cruz,³¹ K. Herner,⁶⁰ G. Hesketh,^{e,43} M.D. Hildreth,⁵³ R. Hirosky,⁷⁸ T. Hoang,⁴⁶ J.D. Hobbs,⁶⁹ B. Hoeneisen,¹¹ M. Hohlfeld,²³ Z. Hubacek,^{9,17} N. Huske,¹⁶ V. Hynek,⁹ I. Iashvili,⁶⁶ Y. Ilchenko,⁷⁶ R. Illingworth,⁴⁷ A.S. Ito,⁴⁷ S. Jabeen,⁷⁴ M. Jaffré,¹⁵ D. Jamin,¹⁴ A. Jayasinghe,⁷² R. Jesik,⁴² P. Jiang,⁶ K. Johns,⁴⁴ M. Johnson,⁴⁷ A. Jonckheere,⁴⁷ P. Jonsson,⁴² J. Joshi,²⁶ A.W. Jung,⁴⁷ A. Juste,³⁹ K. Kaadze,⁵⁶ E. Kajfasz,¹⁴ D. Karmanov,³⁶ P.A. Kasper,⁴⁷ I. Katsanos,⁶³ R. Kehoe,⁷⁶ S. Kermiche,¹⁴ N. Khalatyan,⁴⁷ A. Khanov,⁷³ A. Kharchilava,⁶⁶ Y.N. Kharzheev,³⁴ J.M. Kohli,²⁶ A.V. Kozelov,³⁷ J. Kraus,⁶¹ S. Kulikov,³⁷ A. Kumar,⁶⁶ A. Kupco,¹⁰ T. Kurča,¹⁹ V.A. Kuzmin,³⁶ J. Kvita,⁸ S. Lammers,⁵¹ G. Landsberg,⁷⁴ P. Lebrun,¹⁹ H.S. Lee,³⁰ S.W. Lee,⁵⁴ W.M. Lee,⁴⁷ J. Lellouch,¹⁶ L. Li,⁴⁵ Q.Z. Li,⁴⁷ S.M. Lietti,⁵ J.K. Lim,³⁰ D. Lincoln,⁴⁷ J. Linnemann,⁶¹ V.V. Lipaev,³⁷ R. Lipton,⁴⁷ Y. Liu,⁶ A. Lobodenko,³⁸ M. Lokajicek,¹⁰ R. Lopes de Sa,⁶⁹ H.J. Lubatti,⁷⁹ R. Luna-Garcia,^{f,31} A.L. Lyon,⁴⁷ A.K.A. Maciel,² D. Mackin,⁷⁷ R. Madar,¹⁷ R. Magaña-Villalba,³¹ S. Malik,⁶³ V.L. Malyshev,³⁴ Y. Maravin,⁵⁶ J. Martínez-Ortega,³¹ R. McCarthy,⁶⁹ C.L. McGivern,⁵⁵ M.M. Meijer,³³ A. Melnitchouk,⁶² D. Menezes,⁴⁹ P.G. Mercadante,⁴ M. Merkin,³⁶ A. Meyer,²⁰ J. Meyer,²² F. Miconi,¹⁸ N.K. Mondal,²⁸ G.S. Muanza,¹⁴ M. Mulhearn,⁷⁸ E. Nagy,¹⁴ M. Naimuddin,²⁷ M. Narain,⁷⁴ R. Nayyar,²⁷ H.A. Neal,⁶⁰ J.P. Negret,⁷ P. Neustroev,³⁸ S.F. Novaes,⁵ T. Nunnemann,²⁴ G. Obrant,^{‡,38} J. Orduna,⁷⁷ N. Osman,¹⁴ J. Osta,⁵³ G.J. Otero y Garzón,¹ M. Padilla,⁴⁵ A. Pal,⁷⁵ N. Parashar,⁵² V. Parihar,⁷⁴ S.K. Park,³⁰ J. Parsons,⁶⁷ R. Partridge,^{d,74} N. Parua,⁵¹ A. Patwa,⁷⁰ B. Penning,⁴⁷ M. Perfilov,³⁶ K. Peters,⁴³ Y. Peters,⁴³ K. Petridis,⁴³ G. Petrillo,⁶⁸ P. Pétroff,¹⁵ R. Piegaia,¹ M.-A. Pleier,⁷⁰ P.L.M. Podesta-Lerma,^{g,31} V.M. Podstavkov,⁴⁷ P. Polozov,³⁵ A.V. Popov,³⁷ M. Prewitt,⁷⁷ D. Price,⁵¹ N. Prokopenko,³⁷ S. Protopopescu,⁷⁰ J. Qian,⁶⁰ A. Quadt,²² B. Quinn,⁶² M.S. Rangel,² K. Ranjan,²⁷ P.N. Ratoff,⁴¹ I. Razumov,³⁷ P. Renkel,⁷⁶ M. Rijssenbeek,⁶⁹ I. Ripp-Baudot,¹⁸ F. Rizatdinova,⁷³ M. Rominsky,⁴⁷ A. Ross,⁴¹ C. Royon,¹⁷ P. Rubinov,⁴⁷ R. Ruchti,⁵³ G. Safronov,³⁵ G. Sajot,¹³ P. Salcido,⁴⁹ A. Sánchez-Hernández,³¹ M.P. Sanders,²⁴ B. Sanghi,⁴⁷ A.S. Santos,⁵ G. Savage,⁴⁷ L. Sawyer,⁵⁷ T. Scanlon,⁴² R.D. Schamberger,⁶⁹ Y. Scheglov,³⁸ H. Schellman,⁵⁰ T. Schliephake,²⁵ S. Schlobohm,⁷⁹ C. Schwanenberger,⁴³

R. Schwienhorst,⁶¹ J. Sekaric,⁵⁵ H. Severini,⁷² E. Shabalina,²² V. Shary,¹⁷ A.A. Shchukin,³⁷ R.K. Shivpuri,²⁷ V. Simak,⁹ V. Sirotenko,⁴⁷ P. Skubic,⁷² P. Slattery,⁶⁸ D. Smirnov,⁵³ K.J. Smith,⁶⁶ G.R. Snow,⁶³ J. Snow,⁷¹ S. Snyder,⁷⁰ S. Söldner-Rembold,⁴³ L. Sonnenschein,²⁰ K. Soustruznik,⁸ J. Stark,¹³ V. Stolin,³⁵ D.A. Stoyanova,³⁷ M. Strauss,⁷² D. Strom,⁴⁸ L. Stutte,⁴⁷ L. Suter,⁴³ P. Svoisky,⁷² M. Takahashi,⁴³ A. Tanasijczuk,¹ M. Titov,¹⁷ V.V. Tokmenin,³⁴ Y.-T. Tsai,⁶⁸ K. Tschann-Grimm,⁶⁹ D. Tsybychev,⁶⁹ B. Tuchming,¹⁷ C. Tully,⁶⁵ L. Uvarov,³⁸ S. Uvarov,³⁸ S. Uzunyan,⁴⁹ R. Van Kooten,⁵¹ W.M. van Leeuwen,³² N. Varelas,⁴⁸ E.W. Varnes,⁴⁴ I.A. Vasilyev,³⁷ P. Verdier,¹⁹ L.S. Vertogradov,³⁴ M. Verzocchi,⁴⁷ M. Vesterinen,⁴³ D. Vilanova,¹⁷ P. Vokac,⁹ H.D. Wahl,⁴⁶ M.H.L.S. Wang,⁴⁷ J. Warchol,⁵³ G. Watts,⁷⁹ M. Wayne,⁵³ M. Weber,^{h, 47} L. Welty-Rieger,⁵⁰ A. White,⁷⁵ D. Wicke,²⁵ M.R.J. Williams,⁴¹ G.W. Wilson,⁵⁵ M. Wobisch,⁵⁷ D.R. Wood,⁵⁹ T.R. Wyatt,⁴³ Y. Xie,⁴⁷ C. Xu,⁶⁰ S. Yacoob,⁵⁰ R. Yamada,⁴⁷ S. Yang,⁶ W.-C. Yang,⁴³ T. Yasuda,⁴⁷ Y.A. Yatsunenko,³⁴ Z. Ye,⁴⁷ H. Yin,⁴⁷ K. Yip,⁷⁰ S.W. Youn,⁴⁷ J. Yu,⁷⁵ S. Zelitch,⁷⁸ T. Zhao,⁷⁹ B. Zhou,⁶⁰ J. Zhu,⁶⁰ M. Zielinski,⁶⁸ D. Zieminska,⁵¹ and L. Zivkovic⁷⁴

(The D0 Collaboration*)

¹Universidad de Buenos Aires, Buenos Aires, Argentina

²LAFEX, Centro Brasileiro de Pesquisas Físicas, Rio de Janeiro, Brazil

³Universidade do Estado do Rio de Janeiro, Rio de Janeiro, Brazil

⁴Universidade Federal do ABC, Santo André, Brazil

⁵Instituto de Física Teórica, Universidade Estadual Paulista, São Paulo, Brazil

⁶University of Science and Technology of China, Hefei, People's Republic of China

⁷Universidad de los Andes, Bogotá, Colombia

⁸Charles University, Faculty of Mathematics and Physics,

Center for Particle Physics, Prague, Czech Republic

⁹Czech Technical University in Prague, Prague, Czech Republic

¹⁰Center for Particle Physics, Institute of Physics,
Academy of Sciences of the Czech Republic, Prague, Czech Republic

¹¹Universidad San Francisco de Quito, Quito, Ecuador

¹²LPC, Université Blaise Pascal, CNRS/IN2P3, Clermont, France

¹³LPSC, Université Joseph Fourier Grenoble 1, CNRS/IN2P3,
Institut National Polytechnique de Grenoble, Grenoble, France

¹⁴CPPM, Aix-Marseille Université, CNRS/IN2P3, Marseille, France

¹⁵LAL, Université Paris-Sud, CNRS/IN2P3, Orsay, France

¹⁶LPNHE, Universités Paris VI and VII, CNRS/IN2P3, Paris, France

¹⁷CEA, Irfu, SPP, Saclay, France

¹⁸IPHC, Université de Strasbourg, CNRS/IN2P3, Strasbourg, France

¹⁹IPNL, Université Lyon 1, CNRS/IN2P3, Villeurbanne, France and Université de Lyon, Lyon, France

²⁰III. Physikalisches Institut A, RWTH Aachen University, Aachen, Germany

²¹Physikalisches Institut, Universität Freiburg, Freiburg, Germany

²²II. Physikalisches Institut, Georg-August-Universität Göttingen, Göttingen, Germany

²³Institut für Physik, Universität Mainz, Mainz, Germany

²⁴Ludwig-Maximilians-Universität München, München, Germany

²⁵Fachbereich Physik, Bergische Universität Wuppertal, Wuppertal, Germany

²⁶Panjab University, Chandigarh, India

²⁷Delhi University, Delhi, India

²⁸Tata Institute of Fundamental Research, Mumbai, India

²⁹University College Dublin, Dublin, Ireland

³⁰Korea Detector Laboratory, Korea University, Seoul, Korea

³¹CINVESTAV, Mexico City, Mexico

³²Nikhef, Science Park, Amsterdam, the Netherlands

³³Radboud University Nijmegen, Nijmegen, the Netherlands and Nikhef, Science Park, Amsterdam, the Netherlands

³⁴Joint Institute for Nuclear Research, Dubna, Russia

³⁵Institute for Theoretical and Experimental Physics, Moscow, Russia

³⁶Moscow State University, Moscow, Russia

³⁷Institute for High Energy Physics, Protvino, Russia

³⁸Petersburg Nuclear Physics Institute, St. Petersburg, Russia

³⁹Institució Catalana de Recerca i Estudis Avançats (ICREA) and Institut de Física d'Altes Energies (IFAE), Barcelona, Spain

⁴⁰Stockholm University, Stockholm and Uppsala University, Uppsala, Sweden

⁴¹Lancaster University, Lancaster LA1 4YB, United Kingdom

⁴²Imperial College London, London SW7 2AZ, United Kingdom

⁴³The University of Manchester, Manchester M13 9PL, United Kingdom

⁴⁴University of Arizona, Tucson, Arizona 85721, USA

⁴⁵University of California Riverside, Riverside, California 92521, USA

- ⁴⁶Florida State University, Tallahassee, Florida 32306, USA
⁴⁷Fermi National Accelerator Laboratory, Batavia, Illinois 60510, USA
⁴⁸University of Illinois at Chicago, Chicago, Illinois 60607, USA
⁴⁹Northern Illinois University, DeKalb, Illinois 60115, USA
⁵⁰Northwestern University, Evanston, Illinois 60208, USA
⁵¹Indiana University, Bloomington, Indiana 47405, USA
⁵²Purdue University Calumet, Hammond, Indiana 46323, USA
⁵³University of Notre Dame, Notre Dame, Indiana 46556, USA
⁵⁴Iowa State University, Ames, Iowa 50011, USA
⁵⁵University of Kansas, Lawrence, Kansas 66045, USA
⁵⁶Kansas State University, Manhattan, Kansas 66506, USA
⁵⁷Louisiana Tech University, Ruston, Louisiana 71272, USA
⁵⁸Boston University, Boston, Massachusetts 02215, USA
⁵⁹Northeastern University, Boston, Massachusetts 02115, USA
⁶⁰University of Michigan, Ann Arbor, Michigan 48109, USA
⁶¹Michigan State University, East Lansing, Michigan 48824, USA
⁶²University of Mississippi, University, Mississippi 38677, USA
⁶³University of Nebraska, Lincoln, Nebraska 68588, USA
⁶⁴Rutgers University, Piscataway, New Jersey 08855, USA
⁶⁵Princeton University, Princeton, New Jersey 08544, USA
⁶⁶State University of New York, Buffalo, New York 14260, USA
⁶⁷Columbia University, New York, New York 10027, USA
⁶⁸University of Rochester, Rochester, New York 14627, USA
⁶⁹State University of New York, Stony Brook, New York 11794, USA
⁷⁰Brookhaven National Laboratory, Upton, New York 11973, USA
⁷¹Langston University, Langston, Oklahoma 73050, USA
⁷²University of Oklahoma, Norman, Oklahoma 73019, USA
⁷³Oklahoma State University, Stillwater, Oklahoma 74078, USA
⁷⁴Brown University, Providence, Rhode Island 02912, USA
⁷⁵University of Texas, Arlington, Texas 76019, USA
⁷⁶Southern Methodist University, Dallas, Texas 75275, USA
⁷⁷Rice University, Houston, Texas 77005, USA
⁷⁸University of Virginia, Charlottesville, Virginia 22901, USA
⁷⁹University of Washington, Seattle, Washington 98195, USA

(Dated: November 2, 2011)

We measure the cross section and the difference in rapidities between photons and charged leptons for inclusive $W(\rightarrow l\nu) + \gamma$ production in $e\gamma$ and $\mu\gamma$ final states. Using data corresponding to an integrated luminosity of 4.2 fb^{-1} collected with the D0 detector at the Fermilab Tevatron Collider, the measured cross section times branching fraction for the process $p\bar{p} \rightarrow W\gamma + X \rightarrow l\nu\gamma + X$ and the distribution of the charge-signed photon-lepton rapidity difference are found to be in agreement with the standard model. These results provide the most stringent limits on anomalous $WW\gamma$ couplings for data from hadron colliders: $-0.4 < \Delta\kappa_\gamma < 0.4$ and $-0.08 < \lambda_\gamma < 0.07$ at the 95% C.L.

PACS numbers: 14.80.Bn, 13.85.Rm, 13.85.Qk

The electroweak component of the standard model (SM) has been remarkably successful in describing experimental results. The $WW\gamma$ vertex is one example of self-interactions of electroweak bosons that are a consequence of the non-abelian $SU(2)_L \times U(1)_Y$ gauge symmetry of the SM. In this Letter we use the process

$p\bar{p} \rightarrow W\gamma \rightarrow l\nu\gamma$ ($l = e, \mu$) to study this vertex and to search for any anomalous departure from SM $WW\gamma$ couplings.

An effective Lagrangian parameterizes the $WW\gamma$ couplings with two parameters, κ_γ and λ_γ [1, 2], under the assumptions of electromagnetic gauge invariance, charge conjugation (C), parity (P) and CP conservation. The κ_γ and λ_γ couplings are related to the magnetic dipole and electric quadrupole moments of the W boson [1, 2]. In the SM, $\kappa_\gamma = 1$ and $\lambda_\gamma = 0$, and it is customary to introduce into the notation the difference $\Delta\kappa_\gamma \equiv \kappa_\gamma - 1$.

To assure that the $W\gamma$ cross section does not violate unitarity, a form factor, with a common scale Λ for each non-SM coupling parameter, is introduced to modify the

*with visitors from ^aAugustana College, Sioux Falls, SD, USA, ^bThe University of Liverpool, Liverpool, UK, ^cUPIITA-IPN, Mexico City, Mexico, ^dSLAC, Menlo Park, CA, USA, ^eUniversity College London, London, UK, ^fCentro de Investigacion en Computacion - IPN, Mexico City, Mexico, ^gECFM, Universidad Autonoma de Sinaloa, Culiacán, Mexico, and ^hUniversität Bern, Bern, Switzerland. †Deceased.

terms as $a_0 \rightarrow a_0/(1 + \hat{s}/\Lambda^2)^2$, where $a_0 = \kappa_\gamma, \lambda_\gamma$, and \hat{s} is the square of the partonic center-of-mass energy. In this analysis, the scale Λ is set to 2 TeV. Contributions from anomalous couplings will increase the $W\gamma$ production cross section and yield photons of higher energy than in the SM process[2].

In the SM, tree level production of a photon in association with a W boson occurs due to prompt $W\gamma$ production via the diagrams shown in Fig. 1 or via final state radiation (FSR), where a lepton from the W boson decay radiates a photon. It is an important property of the SM prediction at leading order (LO) that the interference between the amplitudes in Fig. 1 produces a zero in the total $W\gamma$ yield at a specific angle θ^* between the W boson and the incoming quark [3] in the $W\gamma$ rest frame. Since in hadronic collisions the longitudinal momenta of neutrinos from W decay cannot be measured, the angle θ^* at which the radiation amplitude is zero is difficult to measure directly. However, the radiation amplitude zero (RAZ) is also visible in the charge-signed photon-lepton rapidity difference as a dip around $-1/3$ [4].

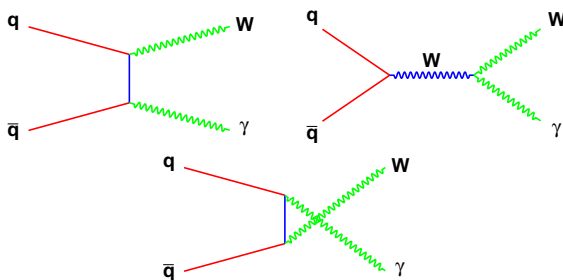


FIG. 1: (color online). Feynman diagrams for prompt $W\gamma$ production.

In this Letter, we present measurements of the cross section and the distribution of the charge-signed photon-lepton rapidity difference for $W\gamma$ production as well as a search for anomalous $WW\gamma$ couplings, using data corresponding to an integrated luminosity of $4.2 \pm 0.3 \text{ fb}^{-1}$ collected by the D0 detector at $\sqrt{s} = 1.96 \text{ TeV}$ at the Fermilab Tevatron Collider. $W\gamma$ production has been studied previously at hadron colliders [5–9]. The latest published D0 result [8] represent the most stringent constraints on anomalous $WW\gamma$ couplings, and include the first study of the charge-signed photon-lepton rapidity difference at a hadron collider. The results of the present analysis provide a significant improvement in the sensitivity to $WW\gamma$ couplings through a nearly factor of six increase in data and by using an artificial neural network for photon identification.

The D0 detector [10] comprises a central tracking system in a 2 T superconducting solenoidal magnet, surrounded by a central preshower (CPS) detector, a liquid-argon sampling calorimeter, and an outer muon system. The tracking system, a silicon microstrip tracker (SMT)

and a scintillating fiber tracker (CFT), provides coverage for charged particles in the pseudorapidity range $|\eta| < 3$ [11]. The CPS is located immediately before the inner layer of the calorimeter, and has about one radiation length of absorber, followed by several layers of scintillating strips. The calorimeter consists of a central sector (CC) with coverage of $|\eta| < 1.1$, and two end calorimeters (EC) covering up to $|\eta| \approx 4.2$. The electromagnetic (EM) section of the calorimeter is segmented into four longitudinal layers (EM*i*, $i = 1, 4$) with transverse segmentation of $\Delta\eta \times \Delta\phi = 0.1 \times 0.1$ [11], except in EM3, where it is 0.05×0.05 . The muon system resides beyond the calorimeter and consists of a layer of tracking detectors and scintillation trigger counters before 1.8 T iron toroidal magnet, followed by two similar layers after the toroid. The coverage of the muon system corresponds to $|\eta| < 2$.

Candidate events with the W boson decaying into an electron and a neutrino are collected using a suite of single-electron triggers. The electrons are selected by requiring an EM cluster in either the CC ($|\eta| < 1.1$) or EC ($1.5 < |\eta| < 2.5$) with transverse energy $E_T > 25 \text{ GeV}$ contained within a cone of radius $\Delta R = \sqrt{(\Delta\eta)^2 + (\Delta\phi)^2} = 0.2$ centered on the axis of the EM shower. At least 90% of the cluster energy must be deposited in the EM section of the calorimeter. In addition, electron candidates are required to be isolated in the calorimeter and in the tracking detector, have a shower shape consistent with that of an electron, and a spatial match to a track. A multivariate likelihood discriminant, which includes information from the spatial track match, must be consistent with that for an electron. An artificial neural network is trained using information from the tracker, calorimeter, and CPS detectors to further reject background from jets misidentified as electrons. The event missing transverse energy, \cancel{E}_T [12], must exceed 25 GeV, and the transverse mass of the W boson, M_T [13], must exceed 50 GeV. To reduce the background from $Z/\gamma^* \rightarrow ee$, where an electron is misidentified as a photon because of tracking inefficiency, the azimuthal angle between the electron and photon is required to be $\Delta\phi_{e\gamma} < 2$.

Candidate events with the W boson decaying into a muon and a neutrino are also collected using a suite of single-muon triggers. The muons are required to be within $|\eta| < 1.6$, isolated in both the tracker and the calorimeter, and matched to a track with transverse momentum $p_T > 20 \text{ GeV}$. To suppress the $Z/\gamma^* \rightarrow \mu\mu$ background, the \cancel{E}_T in the event must exceed 20 GeV, M_T must exceed 40 GeV, and there must be no additional muons or tracks with $p_T > 15 \text{ GeV}$.

The photon candidates in both the electron and muon channels are required to have transverse energy $E_T^\gamma > 15 \text{ GeV}$ within a cone of radius $\Delta R = 0.2$ centered on the EM shower. In addition, photon candidates are required to be either in the CC ($|\eta| < 1.1$) or EC ($1.5 < |\eta| <$

2.5) and must satisfy the following requirements: (i) at least 90% of the cluster energy is deposited in the EM calorimeter; (ii) the calorimeter isolation variable $I = [E_{\text{tot}}(0.4) - E_{\text{EM}}(0.2)]/E_{\text{EM}}(0.2) < 0.15$, where $E_{\text{tot}}(0.4)$ is the total energy in a cone of radius $\Delta R = 0.4$ and $E_{\text{EM}}(0.2)$ is the EM energy in a cone of radius $\Delta R = 0.2$; (iii) the energy-weighted cluster width in the EM3 layer is consistent with that for an EM shower; (iv) the scalar sum of the p_T of all tracks, $p_{T_{\text{trk}}}^{\text{sum}}$, originating from the interaction point in an annulus of $0.05 < \Delta R < 0.4$ around the cluster is less than 2.0 (1.5) GeV for a cluster in the CC (EC); (v) the EM cluster is not spatially matched to either a reconstructed track, or to energy depositions in the SMT or CFT detectors that lie along the trajectory of an electron [14]; and (vi) the output of an artificial neural network (O_{NN}) [15], that combines information from a set of variables sensitive to differences between photons and jets in the tracking detector, the calorimeter, and the CPS detector, is larger than 0.75. To suppress background from FSR, the photon and the lepton must be separated by $\Delta R_{l\gamma} > 0.7$, and the three-body transverse mass [4] of the photon, lepton, and missing transverse energy must exceed 110 GeV. Furthermore, events are accepted only if the $p\bar{p}$ interaction vertex is reconstructed within 60 cm of the center of the D0 detector along the beam axis.

Trigger and lepton identification efficiencies are measured using $Z \rightarrow ll$ ($l = e, \mu$) data. Parts of the photon identification efficiency which rely exclusively on calorimeter information are also determined using $Z \rightarrow ee$ data. The photon track veto efficiencies are determined using $Z \rightarrow l^+l^-\gamma$ events, where the photons are radiated from charged leptons in Z boson decays. The selected data sample is contaminated by the following backgrounds: (i) W +jet events with a jet misidentified as a photon; (ii) “ leX ” events with a lepton, electron, and \cancel{E}_T with the electron misidentified as a photon; (iii) $Z\gamma \rightarrow ll\gamma$ events containing an unidentified lepton; and (iv) $W\gamma \rightarrow \tau\nu\gamma$ events with the τ decaying to e or μ . A Monte Carlo (MC) simulation is used to model the $W\gamma$ signal, as well as the $Z\gamma \rightarrow ll\gamma$ and $W\gamma \rightarrow \tau\nu\gamma$ backgrounds. The signal is simulated using the Baur and Berger LO event generator [2], interfaced to PYTHIA [16] for subsequent parton showering and hadronization. The shape and normalization of the signal E_T^γ spectrum are reweighted to the next-to-leading order (NLO) prediction [4]. The acceptance of the kinematic and geometric requirements for this analysis is calculated using this E_T^γ -weighted signal MC. The $Z\gamma \rightarrow ll\gamma$ and $W\gamma \rightarrow \tau\nu\gamma$ background processes are simulated with PYTHIA. All MC events are generated using the CTEQ6L1 [17] parton distribution functions (PDF), followed by a GEANT [18] simulation of the D0 detector. To accurately model the effects of multiple $p\bar{p}$ interactions and detector noise, data from random $p\bar{p}$ crossings are overlaid on the MC events. The instantaneous luminosity spectrum of these

	$e\nu\gamma$ channel	$\mu\nu\gamma$ channel
W +jet	33.9 ± 3.7	64.6 ± 6.8
leX	1.1 ± 0.6	2.1 ± 0.7
$Z\gamma \rightarrow ll\gamma$	1.8 ± 0.3	17.6 ± 1.9
$W\gamma \rightarrow \tau\nu\gamma$	2.3 ± 0.3	5.4 ± 0.6
Total background	39.1 ± 3.8	89.7 ± 7.2
SM $W\gamma$ prediction	150.9 ± 13.8	282.1 ± 25.4
Data	196	363

TABLE I: Number of predicted and observed events with statistical and systematic uncertainties.

overlaid events is matched to that of the events used in the data analysis. The simulated events are processed using the same reconstruction code that is used for data.

W +jet production is the dominant background for both the electron and muon channels. To estimate this background, the fraction of jets that pass the photon selection criteria but fail either the $p_{T_{\text{trk}}}^{\text{sum}}$ or the shower width requirement, as determined by using a multijet data sample, is parameterized as a function of E_T^γ and η_γ . The background from W +jet production is then estimated starting from an data sample obtained by reversing the requirements either on $p_{T_{\text{trk}}}^{\text{sum}}$ or on shower width requirement, and applying the same parameterization. As a cross-check, the W +jet background is also estimated through a fit to the O_{NN} distribution in data, using MC templates constructed from generated photon and jet events. The result is in good agreement with that obtained from the ratio method. The “ leX ” background is also estimated from an orthogonal data sample by requiring the electron candidate to be matched to a high-quality track. The number of “ leX ” events is obtained by using this orthogonal data sample, taking into account the ratio of the track-matching inefficiency to the track matching efficiency obtained from $Z \rightarrow ee$ data. Events in the electron channel that have both the electron and photon in the EC are excluded from this analysis, because of the poor acceptance for signal and the presence of overwhelming background. The number of predicted and observed events in both the electron and muon channels are summarized in Table I.

The sources of systematic uncertainty that affect the signal acceptance and the background normalization include: integrated luminosity (6.1%), trigger efficiency (5%), electron identification (3%), muon identification (3%), photon identification (3%), track veto (0.9%), signal acceptance due to uncertainties on PDF (0.4%), predicted cross sections for $Z\gamma \rightarrow ll\gamma$ (4%) and $W\gamma \rightarrow \tau\nu\gamma$ (3%), and estimation of W +jet background (10%).

The measured cross sections multiplied by the branching fractions for $\sigma(p\bar{p} \rightarrow W\gamma + X \rightarrow l\nu\gamma + X)$ for photons with $E_T^\gamma > 15$ GeV and $\Delta R_{l\gamma} > 0.7$ are 7.9 ± 0.7 (stat.) ± 0.7 (syst.) pb for the electron channel, and 7.4 ± 0.5 (stat.) ± 0.7 (syst.) pb for the muon

channel. The detector resolution effects that would result in some of the events failing the $E_T^\gamma > 15$ GeV and $\Delta R_{l\gamma} > 0.7$ requirements at the generator level but passing them at the reconstructed-object level have been taken into account. Taking into account the correlation in systematic uncertainties, the combined results yield a cross section multiplied by the branching fraction of 7.6 ± 0.4 (stat.) ± 0.6 (syst.) pb, which is in good agreement with the SM expectation of 7.6 ± 0.2 pb.

The charge-signed photon-lepton rapidity difference for the combination of the two channels is shown in Fig. 2. Because of significant charge mis-identification of EC electrons, only events with CC electrons are used in Fig. 2. The background-subtracted data are in good agreement with the SM prediction, and a χ^2 test comparing the background-subtracted data with the SM prediction yields 4.6 for 11 degrees of freedom.

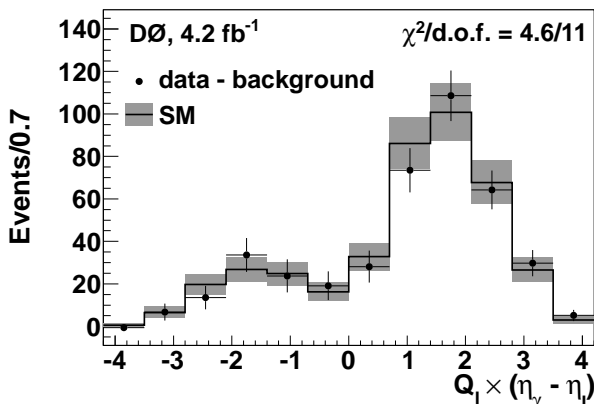


FIG. 2: The charge-signed photon-lepton rapidity difference ($Q_l \times (\eta_\gamma - \eta_l)$, where Q_l is the charge of the lepton) in background-subtracted data compared to the SM expectation for the combined electron and muon channels. The background-subtracted data are shown as black points with error bars representing their total uncertainties. The SM signal prediction is given by the solid line, with the shaded area representing its uncertainty.

The photon E_T^γ distributions in Fig. 3 show good agreement between data and the SM prediction. Therefore, we use the photon E_T^γ spectra to derive limits on anomalous $WW\gamma$ trilinear couplings using a binned likelihood fit to data. The likelihood is calculated assuming Poisson statistics for the number of events in data, the signal, and the background. All systematic uncertainties on sources of background, efficiencies, and luminosity are assumed to be Gaussian, and their correlations are taken into account in the fit. The 95% C.L. limits on the $WW\gamma$ coupling parameters are shown in Fig. 4, with the contour defining the two-dimensional exclusion limits. The one-dimensional 95% C.L. limits are $-0.4 < \Delta\kappa_\gamma < 0.4$ and $-0.08 < \lambda_\gamma < 0.07$, which are obtained by setting one coupling parameter to the SM value and allowing the other to vary.

In summary, we have studied $W\gamma$ production us-

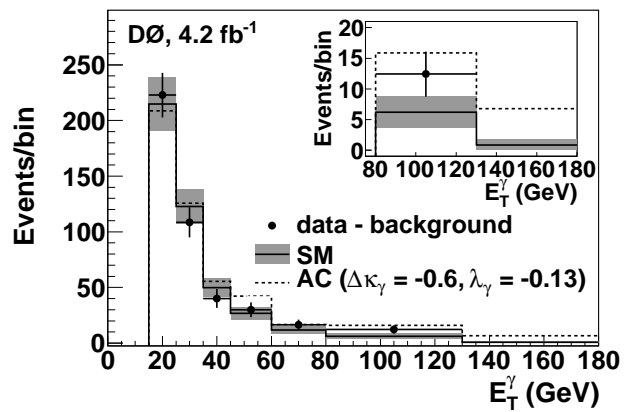


FIG. 3: Photon transverse energy distributions for background-subtracted data compared to the expectation for the SM and for one choice of anomalous couplings for the combined electron and muon channels. The background-subtracted data are shown as black points with uncertainties representing the associated statistical and systematic uncertainties. The SM prediction is given by the solid line, with the shaded area representing its uncertainty. The effect of one example of anomalous couplings is represented by the dashed line. The last E_T^γ bin shows the sum of all events with $E_T^\gamma > 130$ GeV. The inset shows the distributions in the last two bins of E_T^γ .

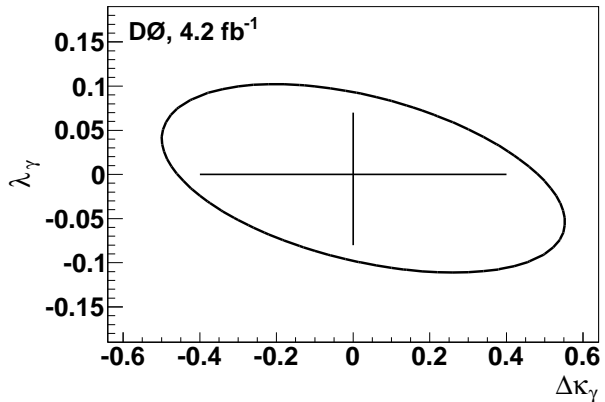


FIG. 4: Limits on the $WW\gamma$ coupling parameters $\Delta\kappa_\gamma$ and λ_γ . The ellipse represents the two-dimensional 95% C.L. exclusion contour. The one-dimensional 95% C.L. limits are shown as the vertical and horizontal lines.

ing data corresponding to an integrated luminosity of 4.2 fb^{-1} collected by the D0 detector at the Fermilab Tevatron Collider. The cross section multiplied by the branching fraction for the process $p\bar{p} \rightarrow W\gamma + X \rightarrow l\nu\gamma + X$ is measured to be 7.6 ± 0.4 (stat.) ± 0.6 (syst.) pb, which is in good agreement with the SM expectation of 7.6 ± 0.2 pb for $E_T^\gamma > 15$ GeV and $\Delta R_{l\gamma} > 0.7$. The distribution of the charge-signed photon-lepton rapidity difference has a minimum near $Q_l \times (\eta_\gamma - \eta_l) = -1/3$, consistent with the SM prediction. We also set the most stringent limits on anomalous $WW\gamma$ couplings at a hadron collider, with the one-dimensional parameters restricted

to $-0.4 < \Delta\kappa_\gamma < 0.4$ and $-0.08 < \lambda_\gamma < 0.07$, at the 95% C.L.

We thank the staffs at Fermilab and collaborating institutions, and acknowledge support from the DOE and NSF (USA); CEA and CNRS/IN2P3 (France); FASI, Rosatom and RFBR (Russia); CNPq, FAPERJ, FAPESP and FUNDUNESP (Brazil); DAE and DST (India); Colciencias (Colombia); CONACyT (Mexico); KRF and KOSEF (Korea); CONICET and UBACyT (Argentina); FOM (The Netherlands); STFC and the Royal Society (United Kingdom); MSMT and GACR (Czech Republic); CRC Program and NSERC (Canada); BMBF and DFG (Germany); SFI (Ireland); The Swedish Research Council (Sweden); and CAS and CNSF (China).

-
- [1] K. Hagiwara *et al.*, Nucl. Phys. **B 282**, 253 (1987).
 [2] U. Baur and E. L. Berger, Phys. Rev. D **41**, 1476 (1990).
 [3] K. O. Mikaelian, Phys. Rev. D **17**, 750 (1978); K. O. Mikaelian, M. A. Samuel, and D. Sahdev, Phys. Rev. Lett. **43**, 746 (1979); R. W. Brown, K. O. Mikaelian, and D. Sahdev, Phys. Rev. D **20**, 1164 (1979).
 [4] U. Baur, T. Han, J. Ohnemus, Rev. D **48**, 5140 (1993); U. Baur, S. Errede and G. Landsberg, Phys. Rev. D **50**, 1917 (1994).
 [5] J. Alitti *et al.* (UA2 Collaboration), Phys. Lett. B **277**, 194 (1992).
 [6] T. Aaltonen *et al.* (CDF Collaboration), Phys. Rev. Lett. **94**, 041803 (2005).
 [7] V. M. Abazov *et al.* (D0 Collaboration), Phys. Rev. D **71**, 091108 (2005).
 [8] V. M. Abazov *et al.* (D0 Collaboration), Phys. Rev. Lett. **100**, 241805 (2008).
 [9] CMS Collaboration, Phys. Lett. B **701**, 535 (2011).
 [10] V. M. Abazov *et al.* (D0 Collaboration), Nucl. Instrum. Methods Phys. Res. A **565**, 463 (2006).
 [11] Pseudorapidity is defined as $\eta = -\ln[\tan(\theta/2)]$, where θ is the polar angle relative to the proton beam direction. ϕ is defined to be the azimuthal angle in the plane transverse to the proton beam direction.
 [12] V. M. Abazov *et al.* (D0 Collaboration), Phys. Lett. B **698**, 6 (2011).
 [13] J. Smith, W. L. van Neerven, and J. A. M. Vermaseren, Phys. Rev. Lett. **50**, 1738 (1983).
 [14] V. M. Abazov *et al.* (D0 Collaboration), Phys. Lett. B **659**, 856 (2008).
 [15] V. M. Abazov *et al.* (D0 Collaboration), Phys. Rev. Lett. **102**, 231801 (2009).
 [16] T. Sjöstrand, S. Mrenna and P. Skands, J. High Energy Phys. **05**, 026 (2006). We use PYTHIA version v6.409 and disable the diagrams corresponding to final state radiation of photons since their contribution is already included in the Baur and Berger event generator.
 [17] J. Pumplin *et al.*, J. High Energy Phys. **07**, 012 (2002); D. Stump *et al.*, J. High Energy Phys. **10**, 046 (2003).
 [18] R. Brun and F. Carminati, CERN Program Library Long Writup W5013 (1993); we use GEANT version v3.21.